

Vision-based hybrid 6-DOF displacement estimation for precast concrete member assembly

Suyoung Choi^{1a}, Wancheol Myeong^{2b}, Yonghun Jeong^{2c} and Hyun Myung^{*1,2}

¹Robotics Program, KAIST, 291 Daehak-ro, Yuseong-gu, Daejeon 34141, Republic of Korea

²Department of Civil and Environmental Engineering, KAIST, 291 Daehak-ro, Yuseong-gu, Daejeon 34141, Republic of Korea

(Received March 21 2017, Revised August 27, 2017, Accepted September 10, 2017)

Abstract. Precast concrete (PC) members are currently being employed for general construction or partial replacement to reduce construction period. As assembly work in PC construction requires connecting PC members accurately, measuring the 6-DOF (degree of freedom) relative displacement is essential. Multiple planar markers and camera-based displacement measurement systems can monitor the 6-DOF relative displacement of PC members. Conventional methods, such as direct linear transformation (DLT) for homography estimation, which are applied to calculate the 6-DOF relative displacement between the camera and marker, have several major problems. One of the problems is that when the marker is partially hidden, the DLT method cannot be applied to calculate the 6-DOF relative displacement. In addition, when the images of markers are blurred, error increases with the DLT method which is employed for its estimation. To solve these problems, a hybrid method, which combines the advantages of the DLT and MCL (Monte Carlo localization) methods, is proposed. The method evaluates the 6-DOF relative displacement more accurately compared to when either the DLT or MCL is used alone. Each subsystem captures an image of a marker and extracts its subpixel coordinates, and then the data are transferred to a main system via a wireless communication network. In the main system, the data from each subsystem are used for 3D visualization. Thereafter, the real-time movements of the PC members are displayed on a tablet PC. To prove the feasibility, the hybrid method is compared with the DLT method and MCL in real experiments.

Keywords: displacement; 6-DOF; vision; Monte Carlo localization (MCL); precast concrete (PC)

1. Introduction

Construction affects many aspects of human life such as the environment, transportation, economy, and other social areas. It requires a huge budget and considerable amount of time. Accordingly, one of the most important issues in the construction industry is reducing construction time. In the past two decades, many studies (Yee and Chuan 2001, Pheng and Chuan 2001) were conducted to reduce construction period. Precast concrete (PC) and prefabricated construction methods have been widely used and are considered promising technologies to address this issue. For bridges, the average lifetime is approximately 50 to 100 years, whereas PC members should be replaced after 10 to 20 years because of live load (Caltrans 2004). Hence, PC members are replaced more than once during the lifetime of a bridge. The replacement of PC members is a burden to the economy and is time consuming. PC technology has led to

significant advancement in manufacturing processes. However, the assembly of PC members still should be improved. Currently, a crane carries a PC member to a particular position, and subsequently, a worker brings it to the required location. In this circumstance, serious accidents can occur. Hence, it is important to develop a method that locates PC members quickly and safely.

In the field of civil engineering, numerous studies on vision sensor-based methods for estimating the displacement of infrastructures were conducted (Park *et al.* 2010, Ji and Chang 2008, Lee and Shinozuka 2006, Wahbeh *et al.* 2003, Olaszek 1999, Marecos *et al.* 1969). These methods are attractive candidates for guiding PC members. However, they are limited to 1D or 2D displacement measurement and cannot measure the 6-DOF (degree of freedom) relative displacement. Recently, several vision or marker-based systems have been introduced to estimate the 6-DOF relative displacement of infrastructures (Myung *et al.* 2011, Jeon *et al.* 2011, Jeon *et al.* 2012, Jeon *et al.* 2013, Jeon *et al.* 2014a, Jeon *et al.* 2014b, Jeon *et al.* 2017). Lee *et al.* (2012, 2014) estimated a 6-DOF relative displacement between a planar marker and a camera using the DLT algorithm. Myeong *et al.* (2014) applied this method to construction members, particularly for the rendezvous of the bridge members. Myeong *et al.* (2015) proposed a Monte Carlo localization (MCL)-based method for estimating the 6-DOF relative displacement of PC members. The DLT method for estimating 6-DOF relative displacement has several drawbacks. One of the problems is

*Corresponding author, Professor

E-mail: hmyung@kaist.ac.kr

^aM.Sc.

E-mail: suyoung.choi@kaist.ac.kr

^bPh.D. Student

E-mail wcmyeong@kaist.ac.kr

^cB.S.

E-mail faceforce@kaist.ac.kr

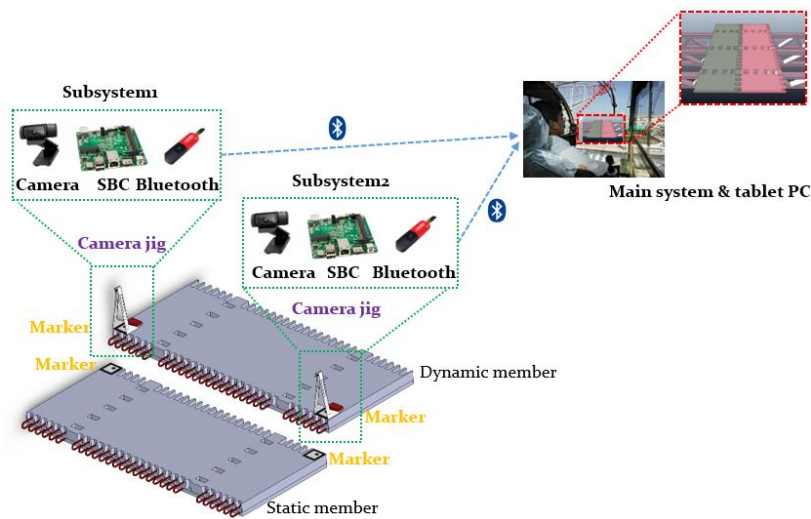


Fig. 1 Multi-marker system and the specifications of its components

that when the marker is partially hidden, the DLT method cannot be employed for calculating the 6-DOF relative displacement because it cannot determine the minimum required number of corner point coordinates of the marker. Second, when the image is blurred, the DLT method cannot be used to determine the corner point coordinates of the marker easily because the image loses sharp shape at the corner of the marker. To overcome these problems, the MCL method is used for the cases where the marker is partially hidden and the image is blurred. However, this method shows some errors even if the image is not blurred because the method is based on the probabilistic localization method using particles. Hence, a hybrid method, which combines the advantages of the DLT method for homography estimation and MCL method, is proposed in this study. The hybrid method selects the 6-DOF relative displacement between the DLT and MCL methods based on which has a more accurate 6-DOF relative displacement.

2. 6-DOF relative displacement estimation with multi-markers

2.1 Multi-marker system for the rendezvous of PC members

The system proposed in this study is developed to estimate the 6-DOF relative displacement of two PC bridge construction members and visualize them with 3D graphics. For the assembly work of the PC members, the basic dimensions of the PC members range from 3 m to 20 m; hence, measuring the displacement of only one spot is insufficient for estimating the overall displacement of the member. Fig. 1 shows the subsystems, main system, and tablet PC of the proposed system. The multi-markers are installed on the static member, which is previously assembled, and the dynamic member, which is carried by the crane. Each subsystem consists of a camera, a single board computer (SBC), and a Bluetooth device. The camera

captures the two markers, and the image processing and estimation of the 6-DOF relative displacement are conducted using the SBC. Generally, the worker of the crane is located approximately 20–30 m from the site of the assembly of the PC members, which is quite far. Hence, the 6-DOF relative displacement is transferred by using wireless technology such as Bluetooth. The main system receives the 6-DOF relative displacement information from the subsystems, and it processes the data for 3D visualization. The tablet PC shows the real-time movement of the PC members based on the 6-DOF relative displacement data for the crane worker. Fig. 2 shows the detailed configuration of the system. Fig. 2(a) represents the subsystems, main system, and tablet PC. The subsystems and main system have modular characteristics, which allow for easy installation at construction sites. The frames of the subsystems are made of a transparent material so that they are less affected by sunshine. Fig. 2(b) shows the markers. The markers have four IDs; IDs 1 and 3 are installed on the static member; IDs 2 and 4 are located on the dynamic member. They have 12 corner points (Q_1, \dots, Q_{12}), and the proposed method measures the more accurate 6-DOF relative displacement than the commonly used four marker corner points based 6-DOF relative displacement estimation such as the April tag (Edwin 2011).

2.2 Visual guidance system

The estimated 6-DOF relative displacement is only a numerical value, and providing real-time guidance information is difficult. Hence, the displacement will be represented using visualization tools, such as 2D or 3D computer graphics, to provide the crane worker with visual aid. As shown in Fig. 3, the visual guidance system is constructed by using a commercial robot simulator called V-REP from Coppelia robotics (2016) to verify the usability. In the program, a 3D-CAD model of the PC bridge members can be imported, and the real-time displacement data simulates the 3D movement.

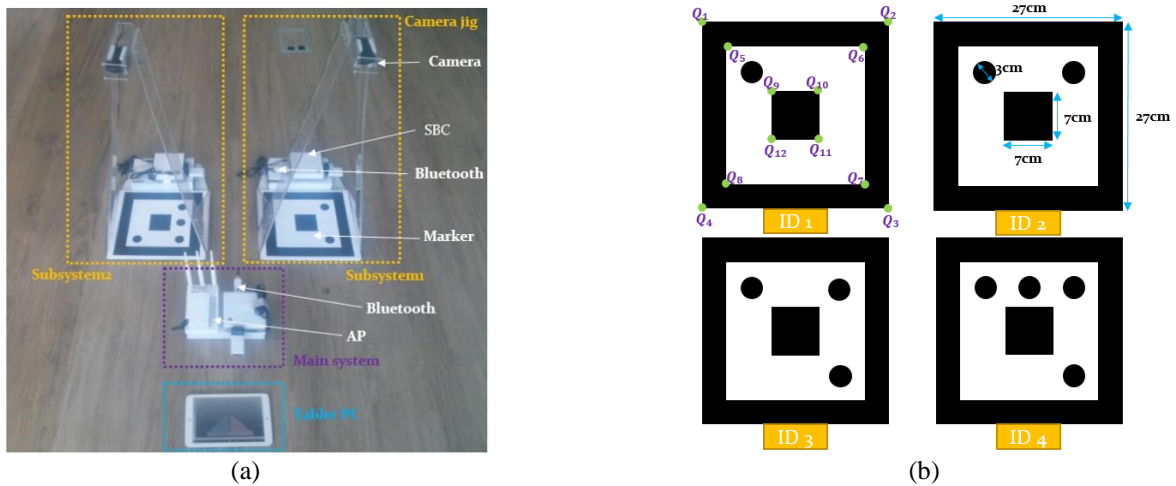


Fig. 2 Detailed configuration of the system. (a) subsystems, main system, and tablet PC and (b) markers

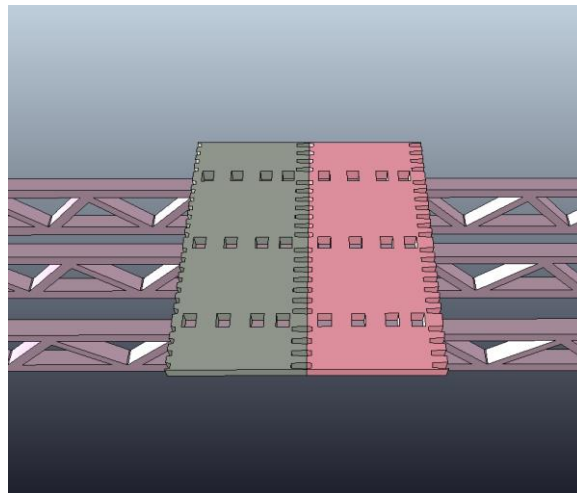


Fig. 3 3D visualization of the PC members

3. Vision sensor and planar marker-based displacement measurement method

3.1 Image processing and marker detection

As shown in Fig. 4, the captured image from the camera is converted from an RGB image to a gray level image. By using a specific threshold value, the gray level image is converted to a binary image wherein a bunch of black and white pixels are connected and grouped through a labeling process. Finally, the square of the marker and the positions of the edge points are extracted with the given geometry of the marker. To increase the accuracy of the position of the corner and displacement measurement results, the extracted corner coordinates with an integer value are refined to a floating value using the subpixel detection algorithm by considering the orthogonal gradient of the intersecting edges (Intel Co. 2015a). For example, at the stage of the

corner point extraction, seen in Fig. 4, the corner point coordinate (q_x^i, q_y^i) ($i = 1, \dots, Q_N$) of the first marker is expressed by an integer type. Q_N is the number of corner points of the marker. However, at the stage of the subpixel extraction, the corner point coordinate is more accurately expressed by a floating type. These image-processing procedures are conducted with an open-source computer vision library such as OpenCV library (Intel Co. 2015a). Traditional camera pose estimation algorithms, such as the DLT direct linear transformation method (Abdel and Karara 1971) and PnP perspective- n -point (Vincent *et al.* 2008), have been used to determine the optimal solution for an extrinsic parameter or homography. This parameter contains information regarding rotational and translational transformations with known intrinsic parameters, the geometry of a landmark, and projected point coordinate parameters.

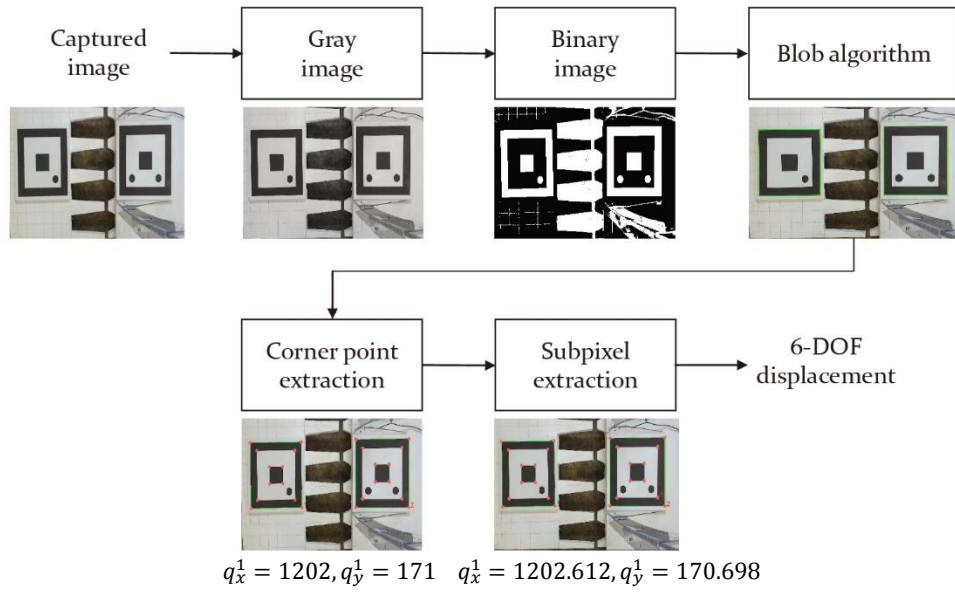


Fig. 4 Procedure of corner point extraction using image processing

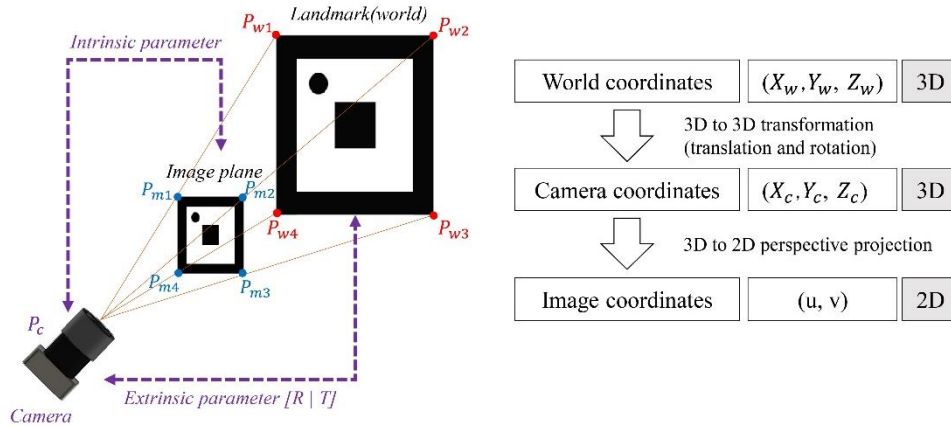


Fig. 5 Camera model and its parameters

3.2 Basic camera model and its pose estimation principle

In the optical model of the camera, the following three coordinate systems exist: camera coordinate, image coordinate, and world coordinate. As shown in Fig. 5, they are related to each other by intrinsic and extrinsic parameters. The intrinsic parameters are the characteristics of the camera, such as focal length, pixel size, and distortion, which can be acquired by using camera calibration algorithms such as Matlab camera calibration app (The Mathworks, Inc. 2015) or GML camera calibration toolbox (Graphics and media lab. 2013).

The extrinsic parameters include rotation and translation transformations between the camera and world coordinates. From the projected image of a specific object with known geometry in the world coordinates, the transformation or

displacement between the camera and object can be calculated by using the following relationship

$$P_m = M_{in} M_{ex} P_w \quad (1)$$

where P_m indicates the coordinate point of the pixel in the image plane, M_{in} is the matrix containing intrinsic parameters, M_{ex} is the matrix containing extrinsic parameters, and P_w is the world coordinate points. The relationship between the marker geometry in the world coordinate and the coordinate in the image plane is employed for evaluating the weight of the MCL in the 2D and 3D image spaces. The following is the expression for the relationship

$$\begin{bmatrix} X_m \\ Y_m \\ Z_m \end{bmatrix} = \begin{bmatrix} -f_x/s_x & 0 & o_x \\ 0 & -f_y/s_y & o_y \\ 0 & 0 & 1 \end{bmatrix} \begin{bmatrix} R_{11} & R_{12} & R_{13} & -R_1 T_r \\ R_{21} & R_{22} & R_{23} & -R_2 T_r \\ R_{31} & R_{32} & R_{33} & -R_3 T_r \end{bmatrix} \begin{bmatrix} X_w \\ Y_w \\ Z_w \end{bmatrix} \quad (2)$$

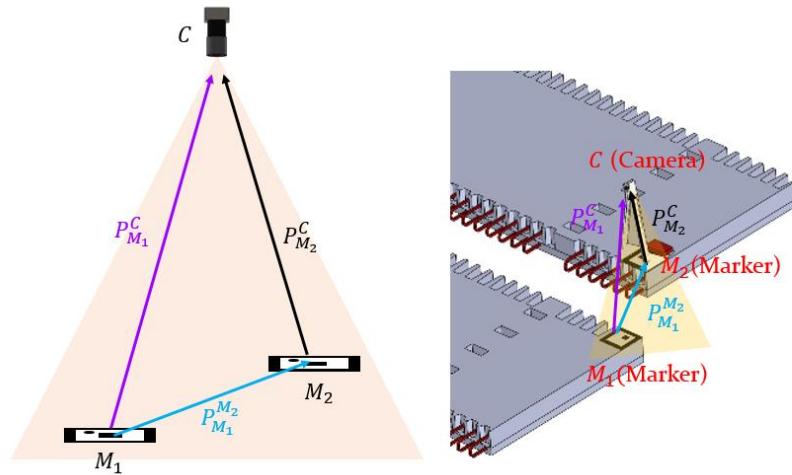


Fig. 6 Relationship between a camera and two markers

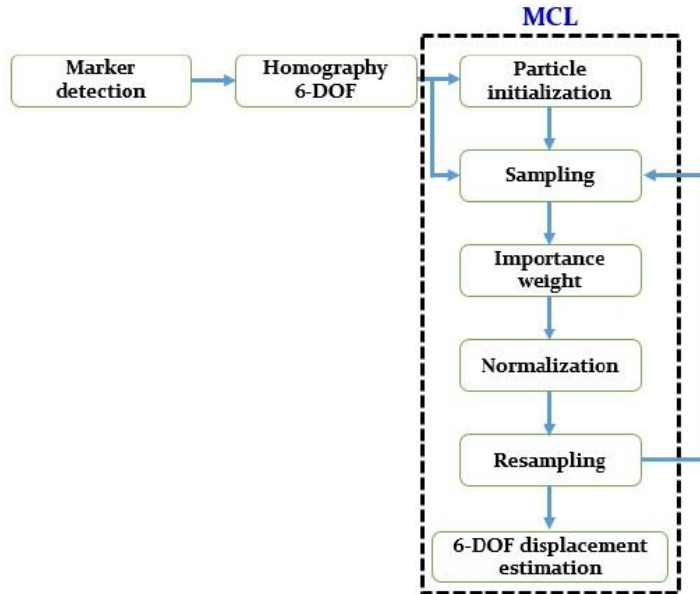


Fig. 7 MCL process

Here, (s_x, s_y) indicates the effective size of the pixels in the horizontal and vertical directions, respectively, (f_x, f_y) are the focal lengths in the horizontal and vertical directions, respectively, and (o_x, o_y) are the principal points in the horizontal and vertical directions, respectively. R_{ij} is the i -th row and j -th column element of the rotation matrix, $R_k = (R_{k1}, R_{k2}, R_{k3})$ ($k = 1, 2, 3$), T_r is the translation vector, (X_m, Y_m, Z_m) are the coordinates of the marker in the image plane, and (X_w, Y_w, Z_w) are the coordinate points of the marker in the world coordinate. Using this equation, the camera pose information with respect to the marker can be estimated. As shown in Fig. 6, to calculate the 6-DOF relative displacement between the two PC members, the following equation is used

$$P_{M_1}^{M_2} = P_{M_1}^C (P_{M_2}^C)^{-1} \quad (3)$$

Here, $P_{M_1}^C$ is the 6-DOF relative displacement of camera C relative to marker M_1 , $P_{M_2}^C$ is the 6-DOF relative displacement of camera C relative to marker M_2 , $P_{M_1}^{M_2}$ is the 6-DOF relative displacement of marker M_1 relative to marker M_2 .

4. Monte Carlo localization (MCL)-based displacement estimation algorithm

4.1 Monte Carlo localization (MCL)

The MCL algorithm is widely used for the localization of a robot in a known environment represented by a map or landmarks (Thrun *et al.* 2001). Using various sensors, a

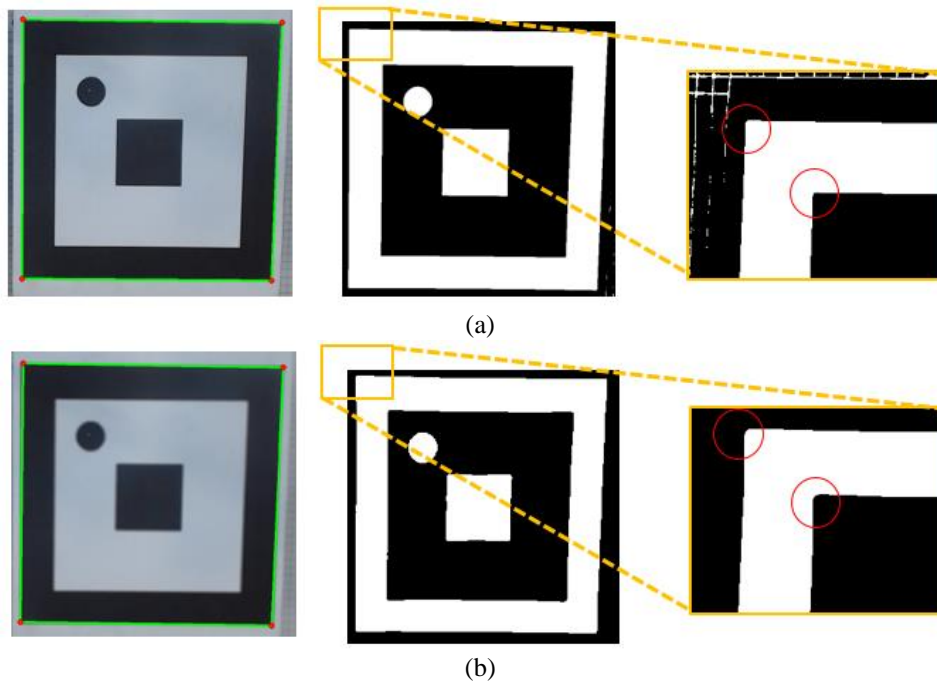


Fig. 8 Marker images. (a) no blurred image, (b) blurred image

robot detects the surrounding environment and estimates its relative pose with respect to the environment. A robot installed with sensors is analogous to the PC member installed with a camera, and the known environment is analogous to the PC member, which is previously assembled and installed with the planar marker. Hence, it is easy to understand the application of the MCL algorithm for estimating the relative displacement between the two members.

The DLT method for homography estimation has two major problems. One of the problems is that when the marker is partially hidden, the DLT method cannot be employed for calculating the 6-DOF relative displacement because it cannot determine the pixel coordinates of the corner points of the marker, which are hidden. The other problem is that when the image is blurred, the corner points of the marker are not accurately detected. Hence, the more the images are blurred, the more inefficient is the DLT method. The MCL can compensate for these problems. The MCL is based on the probability of particles; hence, it can overcome the problems for the case where the pixel coordinates of the corner points of the marker are not exactly extracted.

As shown in Fig. 7, the MCL process has several steps. The first step is particle initialization, where the particles are generated randomly. Second, the sampling step calculates the particles using a motion model. Thereafter, the importance weight step assigns weights to the particles depending on which one is more reliable. In the normalization step, the weights of the particles are adjusted

with the common scale such that the sum of the weights of the particles is equal to 1. In the resampling stage, the particles with low weights are replaced by the new particles, and the new particles are generated nearby particles which have high weights.

4.2 MCL process

In the particle initialization step, particles $\mathbf{x}_n^{(0)}$, $n=(1, \dots, N)$ (N : total number of particles) are randomly generated with normal distribution from the 6-DOF relative displacement, which is calculated by using the DLT method $\mathbf{h}^{(0)}$, shown in Algorithm 1. In the sampling step, particles $\mathbf{x}_n^{(t)}$ are reflected with motion model $\Delta \mathbf{h}^{(t)}$, which is the difference between $\mathbf{h}^{(t)}$ and $\mathbf{h}^{(t-1)}$.

In the importance weight step, the generated particles cannot be considered as actual measurement, but only as a candidate for the measurement; an evaluation process is necessary to determine whether each particle can be retained. As shown in Fig. 8, when the image is blurred, the pixel coordinate of the corner points of the marker is not accurately detected; hence, it is not directly used for calculating the importance weight in the MCL process. Instead of this pixel coordinate, as shown in Fig. 9 and Algorithm 1, the score value is measured, which is the average distance between the pixel points (represented by blue dots) induced by the particles and other pixel points (represented by red dots) on the side of the marker (Yuko and Hideo 2007). $p_{s,n}^{(t)}$, $p_{s+1,n}^{(t)}$, $s = (1, 2, 3)$ (s : the order of the corner points of the marker) are the pixel coordinates of the corner points of the marker reprojected from the

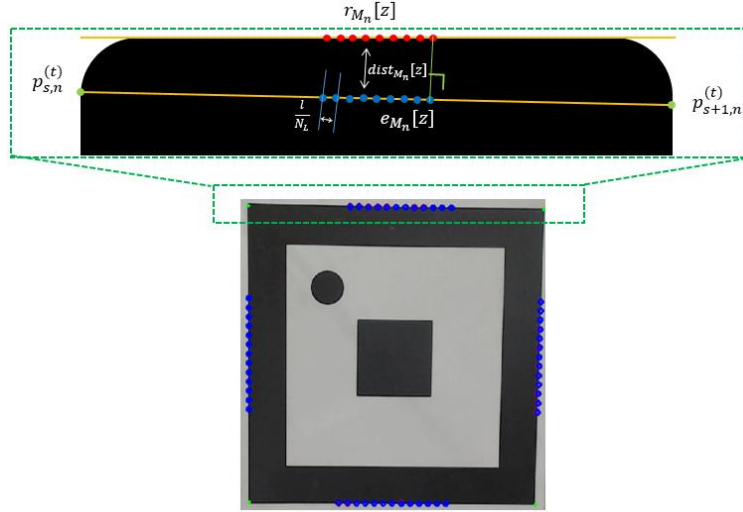


Fig. 9 Calculating score value

Algorithm 1 MCL algorithm

```

1: function MCL( $\mathbf{h}^t$ )
2:    $\mathbf{x}_{1,\dots,N}^{(0)} = \mathbf{h}^{(0)} + \text{normal distributed } rand()$ ; ▷ Particle initialization
3:    $\mathbf{w}_{1,\dots,N}^{(0)} = 1/N$ ;
4:   for  $n = 1$  to  $N$  do
5:      $\mathbf{x}_n^{(t)} = \mathbf{x}_n^{(t-1)} + \Delta \mathbf{h}^{(t)}$ ; ▷ Sampling
6:     for  $z = 1$  to  $N_C$  do
7:        $dist_{M_n}[z] = \text{Euclidean distance between } r_{M_n}[z] \text{ and } e_{M_n}[z]$ ;
8:        $totalDist_{M_n} = totalDist_{M_n} + dist_{M_n}[z]$ ;
9:     end for
10:     $avgDist_{M_n} = totalDist_{M_n} / N_C$ ; ▷ Calculating score value
11:     $\mathbf{w}_n^{(t)} \propto \exp(-(avgDist_{M_n})^2 / 2\sigma^2) / \sqrt{2\pi\sigma^2}$ ; ▷ Importance weight
12:     $\hat{\mathbf{w}}_n^{(t)} = \frac{w_n^{(t)}}{\sum_{k=1}^N w_n^{(k)}}$ ; ▷ Normalization
13:  end for
14:   $N_{eff} = [\sum_{k=1}^N (\hat{w}_k^{(t)})^2]^{-1}$ 
15:  if  $N_{eff} \leq \eta_{eff}$  then
16:     $u_j = ((j-1) + \hat{u}_j) / N$  with  $\hat{u}_j \sim \text{UniformRandom}(0, 1)(j = 1, \dots, N)$ 
17:     $\backslash\backslash u_j$  is ordered random numbers.
18:    if  $u_j \in (\sum_{s=1}^{i-1} \hat{w}_s^{(t)}, \sum_{s=1}^i \hat{w}_s^{(t)}) (i = 1, \dots, N)$  then  $\mathbf{x}_i \rightarrow \mathbf{x}_j$  ▷ Systematic resampling
19:     $\backslash\backslash \mathbf{x}_j$  is resampled particles.
20:  end if
21: end if
22:  $\mathbf{P}_M^{(t)}$  is calculated from average of  $N_R$  particles. ▷ 6-DOF displacement based on MCL
23: return  $\mathbf{P}_M^{(t)}$ 
24: end function

```

articles using the camera model. $e_{M_n}[z]$, $z = (1, \dots, N_C)$ (N_C : the total number of points on visible lines which connect points $p_{s,n}^{(t)}$ and $p_{s+1,n}^{(t)}$ on a marker) are points which are located at the center of the line. $e_{M_n}[z]$ has the same distance of l/N_L with an adjacent point on the line where l is the length of the line and N_L is the number of the points located at the center part of the line. $r_{M_n}[z]$ (red dots) is the point from the foot of the perpendicular drawn from $e_{M_n}[z]$, and it is on the side of the marker. Finally, the score value is the average distance $avgDist_{M_n}$ between $e_{M_n}[z]$ and $r_{M_n}[z]$. The smaller the average distance, the higher

the weight of the particle. The next step is normalization. The weights of the particles are modified with the common scale such that the sum of the weights of the particles is equal to 1. The particles are resampled when the effective number of particles, N_{eff} , is less than or equal to a threshold η_{eff} . In the resampling step, the particles with low weights are replaced by the new particles, and the new particles are generated as from the particles having high weights by using systematic resampling.

Table 1 Notation in Algorithm 1

Symbol	Meaning
t	Time
N_R	Number of representative particles having high weights in resampling step
$\mathbf{w}_n^{(t)}$	Weights of particles at time t
$\hat{\mathbf{w}}_n^{(t)}$	Normalized weights of particles at time t
$dist_{M_n}[z]$	Euclidean distance between $r_{M_n}[z]$ and $e_{M_n}[z]$
$totalDist_{M_n}$	Sum of distances $dist_{M_n}[z]$
$\mathbf{x}_j^{(t)}$	Representative particles having high weights in resampling step
$\mathbf{x}_{j+k}^{(t)}$	Resampled particles
$\mathbf{P}_M^{(t)}$	6-DOF displacement from MCL

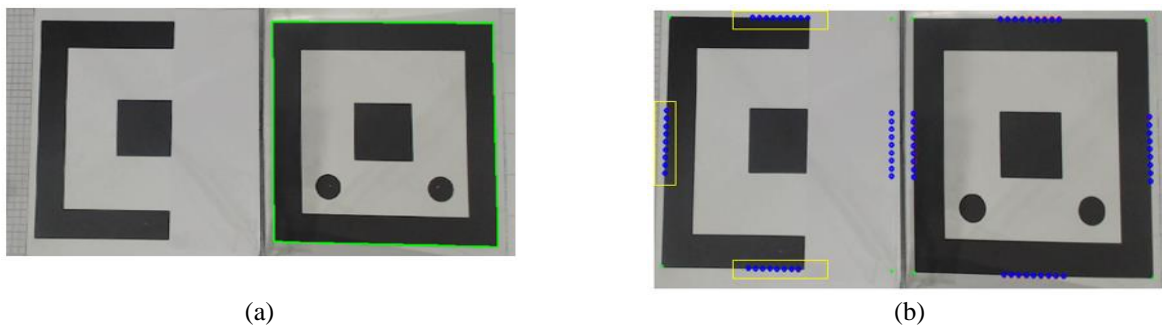


Fig. 10 Comparison when the marker is partially hidden. (a) The DLT method for homography estimation and (b) MCL

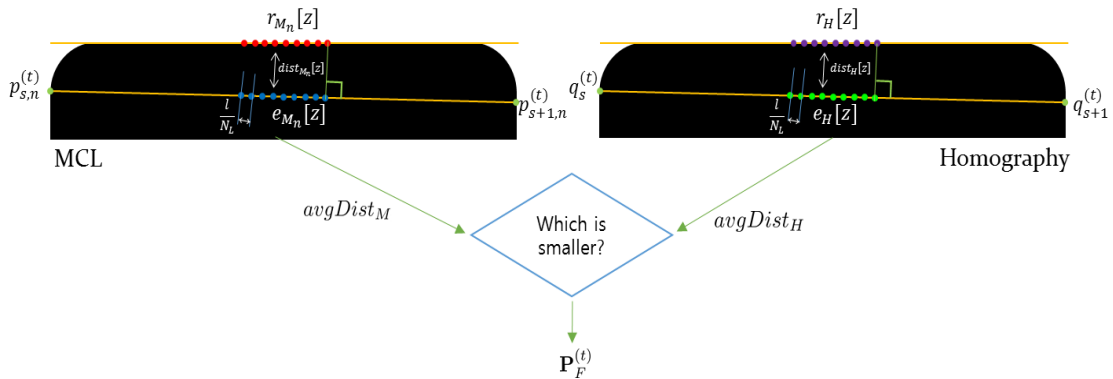


Fig. 11 Process for choosing the final 6-DOF relative displacement

5. Hybrid method

The hybrid method is employed for combining the advantages of the DLT and MCL methods. As shown in Fig. 10(a), when the marker is partially hidden, some corner points of the marker are not detected. Thus, the DLT method cannot calculate 6-DOF relative displacement between one and the other marker. However, the MCL method can estimate 6-DOF relative displacement even with partial occlusion. If particles have 6-DOF relative

displacement information, though the marker is partially hidden, the MCL can determine importance weight from the visible side of the marker (yellow boxes in Fig. 10(b)). Hence, the MCL can calculate the 6-DOF relative displacement even when the marker is partially hidden. The overall procedure for the hybrid algorithm is shown in Algorithm 2. As shown in Algorithm 2, 6-DOF relative displacement induced by MCL $\mathbf{P}_M^{(t)}$ is chosen for the final 6-DOF relative displacement $\mathbf{P}_F^{(t)}$.

In addition, the hybrid method is used when the marker image is blurred. When the marker image is blurred, the

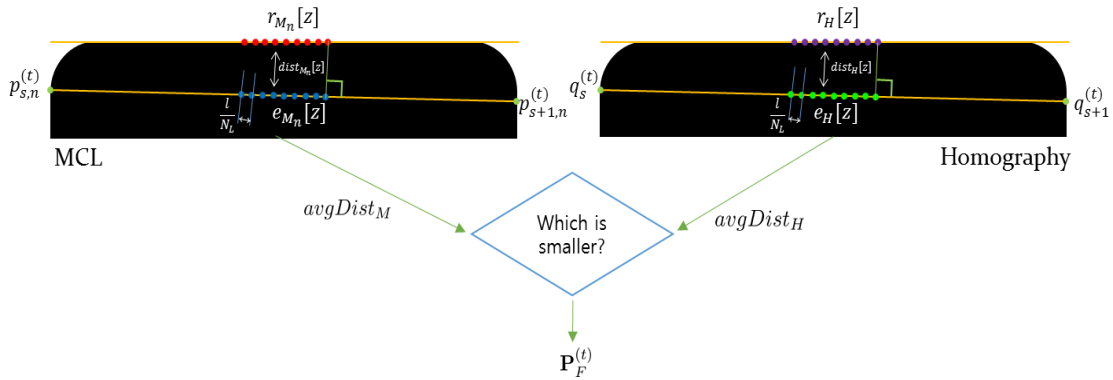


Fig. 11 Process for choosing the final 6-DOF relative displacement

Algorithm 2 Hybrid algorithm

```

1: function HYBRID(bDetected, avgDistM,  $\mathbf{q}_s^{(t)}$ ,  $\mathbf{P}_H^{(t)}$ ,  $\mathbf{P}_M^{(t)}$ )
2:   for  $z = 1$  to  $N_C$  do
3:      $dist_H[z] =$  Euclidean distance between  $r_H[z]$  and  $e_H[z]$ ;
4:      $totalDist_H = totalDist_H + dist_H[z]$ ;
5:   end for
6:    $avgDist_H = totalDist_H / N_C$ ;
7:   if  $bDetected == \text{true}$  then
8:     if  $avgDist_M \geq avgDist_H$  then
9:        $\mathbf{P}_F^{(t)} = \mathbf{P}_H^{(t)}$ ;
10:    else
11:       $\mathbf{P}_F^{(t)} = \mathbf{P}_M^{(t)}$ ;
12:    end if
13:  else
14:     $\mathbf{P}_F^{(t)} = \mathbf{P}_M^{(t)}$ ;
15:  end if
16:  return  $\mathbf{P}_F^{(t)}$ 
17: end function

```

DLT method has more error because it cannot accurately detect the corner points of the marker. However, the MCL can estimate 6-DOF relative displacement more accurately than the DLT method when the marker image is blurred. As shown in Fig. 11, to determine the more useful method for estimating the 6-DOF relative displacement, the average distances obtained from the MCL and the DLT methods are compared for determining the smaller value. $avgDist_M$ is the average distance which is induced from the particle having the highest weight. $avgDist_H$ is the average distance from the corner points $q_x^{(t)}$, $q_{s+1}^{(t)}$, $s = (1, 2, 3)$ (s : the order of the corner points of the marker) of the marker in the DLT method. Finally, as shown in Algorithm 2, if the marker is visible and detected ($bDetected = \text{true}$), the final 6-DOF relative displacement is decided from the process as illustrated in Fig. 11. If the marker is partially hidden, the MCL is chosen for the final 6-DOF relative displacement.

6. Experimental tests

6.1 6-DOF relative displacement estimation with no blurred image

This experiment is conducted for verifying the performance of only the DLT method when the image is not blurred. Fig. 12 shows the configuration of the experimental system. The dynamic member is the PC member which is carried by the crane, and the static member is the PC member which is installed in advance. The camera jig is on the dynamic member and it is moved by the motorized motion-stage (Thorlabs, 2015) to measure the ground truth. The stage helps provide artificial translation and rotation movement to the dynamic member using the camera jig.

The camera is HD pro webcam C920 from Logitech with a frame rate of 30 Hz and a resolution of 1920×1080 pixels.

Table 2 Notation in Algorithm 2

Symbol	Meaning
$bDetected$	If a marker is detected, $bDetected = true$, otherwise $bDetected = false$
$e_H [z]$	The points located at the center of the line which connects $q_s^{(t)}$ and $q_{s+1}^{(t)}$
$r_H [z]$	The point from the foot of the perpendicular drawn from $e_H [z]$
$dist_H [z]$	Euclidean distance between $r_H [z]$ and $e_H [z]$
$totalDist_H$	Sum of distances $dist_H [z]$
$\mathbf{P}_H^{(t)}$	6-DOF displacement from the DLT method

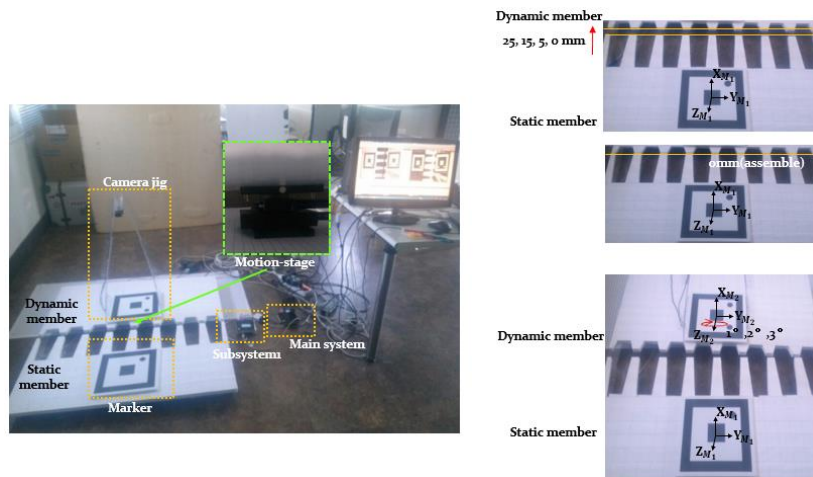


Fig. 12 Overall setup for experimental tests

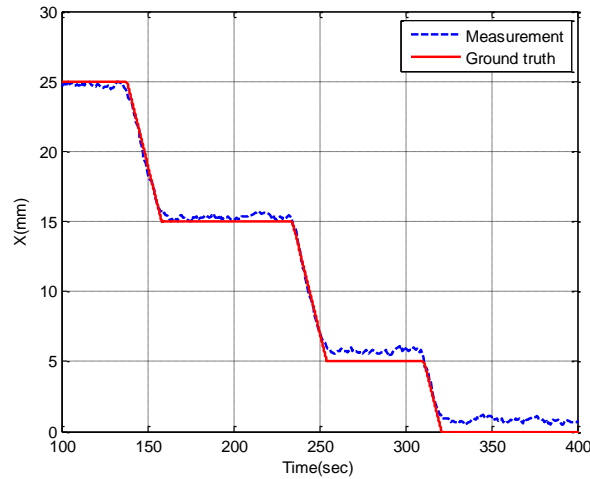


Fig. 13 Graph obtained from experimental result for translation movement along the X-axis

The SBC is NUC5i3RYK from Intel, which has a core i3 processor (Intel Co. 2015b). The main system receives the 6-DOF relative displacement information from the subsystems. The distance between the cameras and markers is 70 cm. The Bluetooth device is parani-UD100 from SENA and has a maximum transfer rate of 3 Mbps, capable of obtaining data from a maximum distance of 300 m from

a transmission spot (SENA CO. 2015). The dynamic member is installed on the motion-stage and moves linearly for 25 mm, 15 mm, 5 mm, and 0 mm along the X-axis, and rotates 0°, 1°, 2°, and 3° about the Z-axis. The experiment is repeated thrice.

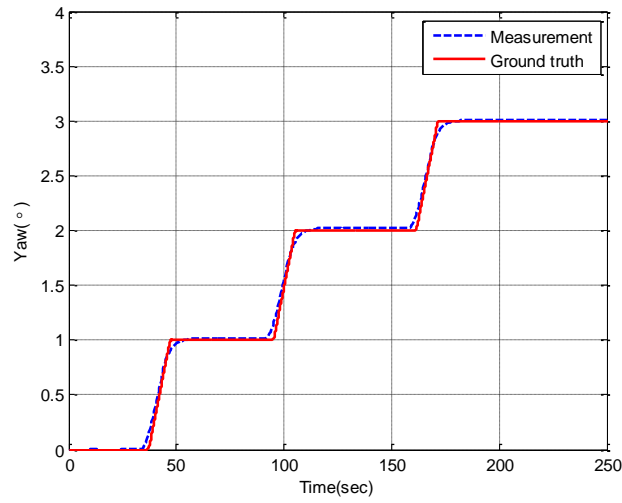


Fig. 14 Graph obtained from experimental result for rotation movement about the Z-axis

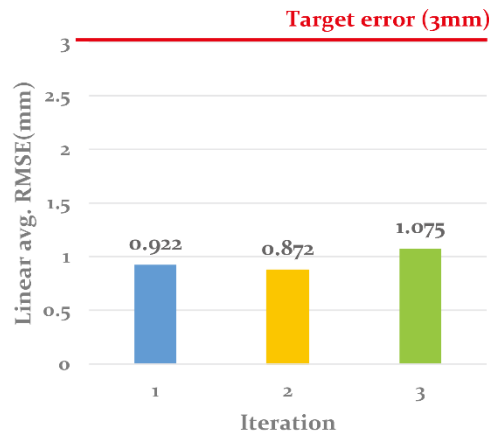


Fig. 15 Experimental average of linear RMSE graph of translation movement at 0 mm along the X-axis

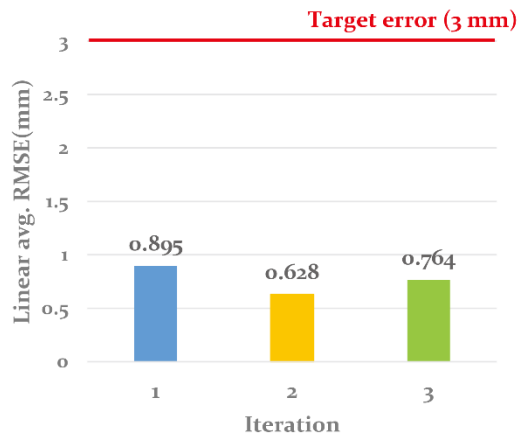


Fig. 16 Experimental average of linear RMSE graph of rotation movement at 3° about the Z-axis

Table 3 RMSE with translation movement along X-axis. Linear avg. is average RMSE in X, Y, and Z axes. Angular avg. is the average RMSE of roll, pitch, and yaw

Iteration	Distance (mm)	X(mm)	Y(mm)	Z(mm)	Linear avg. (mm)	Roll(°)	Pitch (°)	Yaw(°)	Angular avg.(°)
1	25	0.301	0.518	0.400	0.721	0.036	0.028	0.023	0.029
	15	0.345	0.424	0.183	0.576	0.013	0.028	0.047	0.029
	5	0.755	0.354	0.123	0.844	0.016	0.053	0.067	0.045
	0	0.865	0.300	0.106	0.922	0.062	0.065	0.123	0.083
2	25	0.180	0.303	0.211	0.410	0.019	0.017	0.008	0.015
	15	0.468	0.500	0.086	0.690	0.048	0.035	0.020	0.034
	5	0.507	0.672	0.113	0.849	0.081	0.035	0.051	0.056
	0	0.704	0.494	0.144	0.872	0.102	0.044	0.095	0.080
3	25	0.330	0.301	0.210	0.494	0.022	0.255	0.009	0.019
	15	0.163	0.795	0.320	0.872	0.081	0.010	0.047	0.046
	5	0.599	0.662	0.609	1.086	0.085	0.045	0.075	0.069
	0	0.675	0.521	0.658	1.075	0.113	0.048	0.130	0.097

Table 4 RMSE with rotation movement about Z-axis. Linear avg. is average RMSE in X, Y, and Z axes. Angular avg. is the average RMSE of roll, pitch, and yaw

Iteration	Angle (°)	X(mm)	Y(mm)	Z(mm)	Linear avg. (mm)	Roll (°)	Pitch (°)	Yaw (°)	Angular avg.(°)
1	0	0.154	0.435	0.132	0.479	0.034	0.012	0.002	0.016
	1	0.287	0.651	0.243	0.752	0.050	0.051	0.013	0.038
	2	0.269	0.528	0.299	0.644	0.045	0.065	0.014	0.041
	3	0.348	0.801	0.194	0.895	0.063	0.071	0.015	0.050
2	0	0.059	0.204	0.103	0.236	0.015	0.005	0.002	0.007
	1	0.142	0.164	0.337	0.401	0.014	0.042	0.011	0.022
	2	0.587	0.148	0.720	0.941	0.007	0.095	0.012	0.038
	3	0.471	0.087	0.40	0.628	0.006	0.083	0.005	0.031
3	0	0.427	0.283	0.208	0.553	0.025	0.038	0.004	0.022
	1	0.057	0.260	0.220	0.345	0.02	0.038	0.018	0.025
	2	0.122	0.085	0.623	0.640	0.006	0.071	0.022	0.033
	3	0.714	0.221	0.163	0.764	0.018	0.047	0.011	0.025

As shown in Figs. 13 and 14, the blue dashed line indicates the DLT method and the red solid line indicates the ground truth. The target error of 3 mm is the maximum error of the assembly of the two PC members, which is determined through discussions with bridge engineers. Figs. 15 and 16 are the average of linear Root Mean Square Error (RMSE) graph at 0 mm along the X-axis and at 3° about Z-axis. The more important RMSE is the closest case (0 mm, 3°) when the two PC members are just before the match.

Tables 3 and 4 give the RMSE related to the linear translation and rotation, respectively. In the translation case, the maximum linear RMSE is 1.075 m at 0 mm along the X-axis. For the rotation case, the maximum linear RMSE is 0.895 m at 3° about the Z-axis below the target error of 3 mm.

6.2 6-DOF relative displacement estimation with blurred image

To assume that blurring occurred for the situation where the assembly of the member is almost complete, the image

was blurred at 5 mm in the X-axis direction. The blurring provided is a Gaussian blur and when blurring occurs randomly from standard deviation of 0 to 5 pixels, the DLT and MCL methods are combined. The DLT, MCL, and hybrid methods are then compared with the ground truth. The constants are set to $N = 200$, $N_R = 20$, and $N_L = 9$. Fig. 17 shows the results. The blue dashed line, black dash-dotted line, green dotted line, and red solid line indicate the results from the DLT method, MCL method, hybrid method, and the ground truth, respectively. The hybrid method employs the 6-DOF relative displacement from the DLT or MCL depending on which has the lower average distance, as shown in Algorithm 2. When blurring increases, error in the DLT method generally increases, but the MCL method is somewhat steady. However, in the small blurred image, the DLT method more accurately estimates the 6-DOF relative displacement than the MCL. Hence, the displacement is more accurately measured by using the hybrid method compared to the DLT method or MCL method alone, as shown in Table 5.

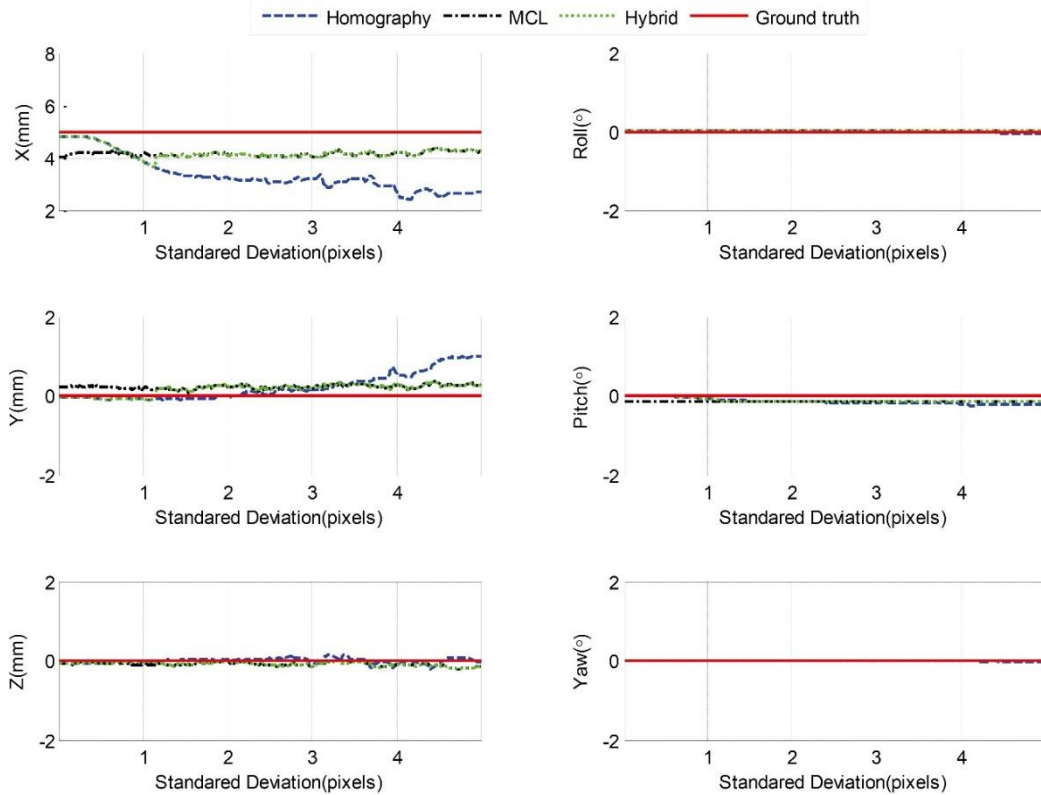


Fig. 17 Result of DLT, MCL, hybrid methods, and ground truth according to blurring

Table 5 RMSE with DLT, MCL, and hybrid method when the image is blurred. Linear avg. is average RMSE in X, Y, and Z axes, Angular avg. is the average RMSE of roll, pitch, and yaw

Method	X(mm)	Y(mm)	Z(mm)	Linear avg.(mm)	Roll (°)	Pitch (°)	Yaw (°)	Angular avg.(°)
DLT	1.525	0.351	0.061	1.566	0.020	0.137	0.014	0.057
MCL	0.729	0.197	0.085	0.760	0.022	0.119	0.013	0.051
Hybrid	0.711	0.180	0.085	0.739	0.021	0.106	0.013	0.047

Table 6 RMSE with DLT, MCL, and hybrid method when the marker is occluded. Linear avg. is average RMSE of X, Y, and Z axes. Angular avg. is the average RMSE of roll, pitch, and yaw

Method	X(mm)	Y(mm)	Z(mm)	Linear avg.(mm)	Roll (°)	Pitch (°)	Yaw (°)	Angular avg.(°)
DLT				N/A				
MCL	0.447	0.269	0.092	0.531	0.024	0.027	0.010	0.020
Hybrid	0.296	0.151	0.108	0.350	0.020	0.024	0.009	0.018

6.3 6-DOF relative displacement estimation with a partially hidden marker

Initially, the marker was visible, and after approximately 31 s, the marker is partially occluded, as shown in Fig. 10. As shown in Fig. 10(b), when the marker is partially hidden, the DLT method cannot calculate 6-DOF relative displacement because it cannot determine the pixel coordinates of the corner points of the marker; hence, the 6-DOF relative displacement is not estimated, which implies

that the DLT method cannot calculate the displacement, as shown in Fig. 18. However, the MCL method can estimate the 6-DOF relative displacement because the particles have the 6-DOF relative displacement information and the importance weights can be determined from the visible side of the marker. Hence, the hybrid method employs the 6-DOF relative displacement obtained from the MCL method when the marker is partially hidden. Fig. 18 shows the result. The blue dashed line, black dash-dotted line, green dotted line, and red solid line indicate the results from the

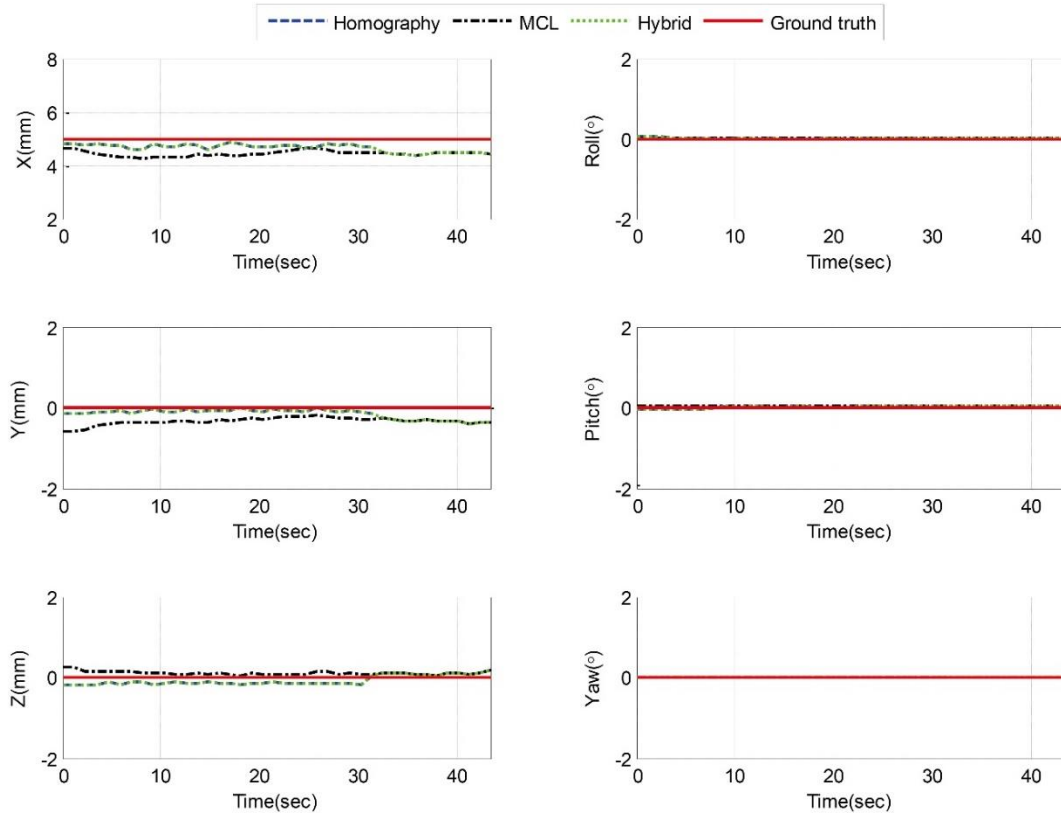


Fig. 18 Result of DLT, MCL, hybrid method, and ground truth when the marker is occluded

Table 7 Comparing ground truth and measurement from subsystems

Systems	Items	X(mm)	Y(mm)	Z(mm)	Linear avg.(mm)
Sub-system1	Ground truth	640.88	30.87	6.12	
	Measurement	639.21	31.20	6.29	1.71
	Error	1.67	-0.33	-0.17	
Sub-system2	Ground truth	623.42	28.27	4.58	
	Measurement	622.01	27.12	4.23	1.85
	Error	1.41	14.15	0.35	

DLT, MCL, hybrid method, and the ground truth, respectively. In Table 6, RMSE of the DLT method is not available because the DLT method cannot estimate 6-DOF relative displacement when the marker is partially hidden. The hybrid method calculates the displacement more accurately than the DLT or MCL method alone, as shown in Table 6.

6.4 Field test

A field test was conducted at the MUNAM bridge, Muju, Jeollabuk-do, Republic of Korea. The length of the bridge is 36 m. As shown in Fig. 19, the length of the PC member used for the bridge is 5 m, and the width is 1.6 m. Fig. 20 shows the process of construction of the bridge using the PC members. A PC member is moved by the crane on a girder and it is closely assembled next to another PC member to make the bridge

strong and elaborate.

As shown in Fig. 21, the camera jigs are installed on both sides of the dynamic member which is carried by the crane, and the markers are set on the static member which is previously assembled. Fig. 22 shows the 3D visualization of the PC members, looked at by the crane worker. The dynamic member moves with the 6-DOF relative displacement information of the PC members, which is calculated from multiple cameras and markers. The crane worker can assemble the two PC members quickly and accurately using the 3D visualization of the PC members. As shown in Fig. 23, the measurement error is calculated when the PC member is completely assembled. Subsystem1 and Subsystem2 have linear average errors of 1.71 mm and 1.85 mm, respectively as shown in Table 7. Hence, the proposed 6-DOF relative displacement method has error within a few millimeters.

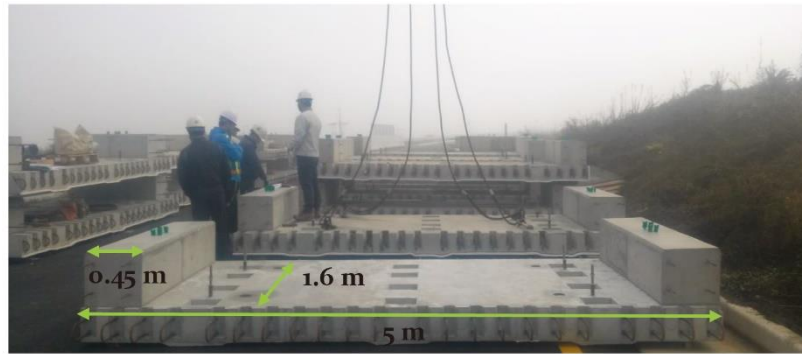


Fig. 19 Dimensions of the PC member



Fig. 20 Assembly process of PC members



Fig. 21 Setting camera jigs and markers

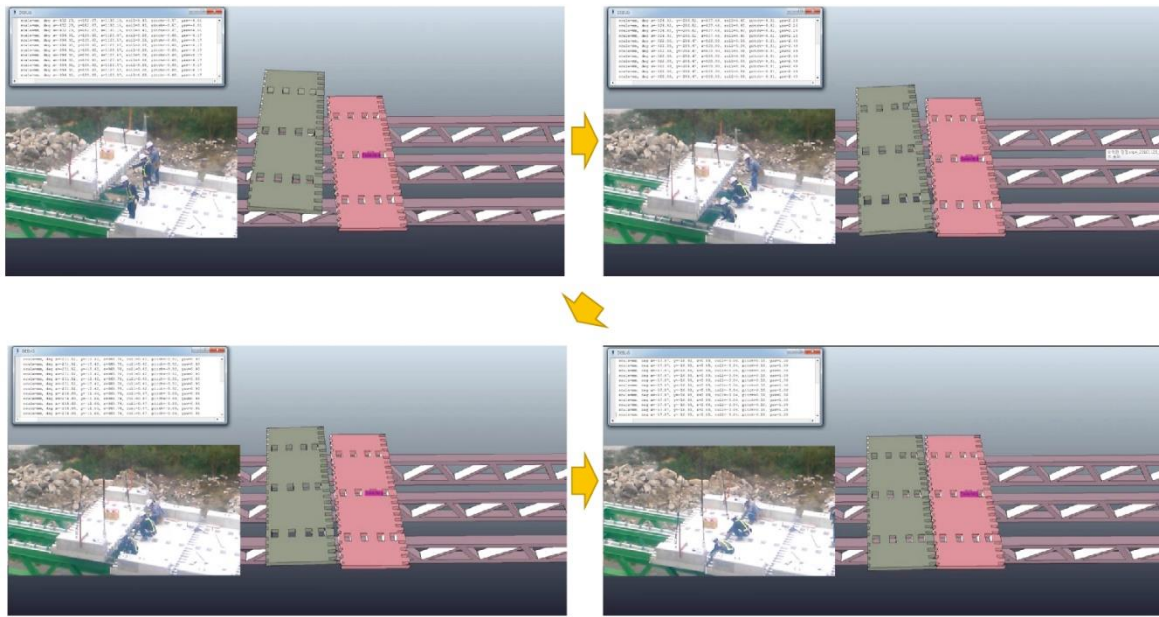


Fig. 22 3D visualization of PC members

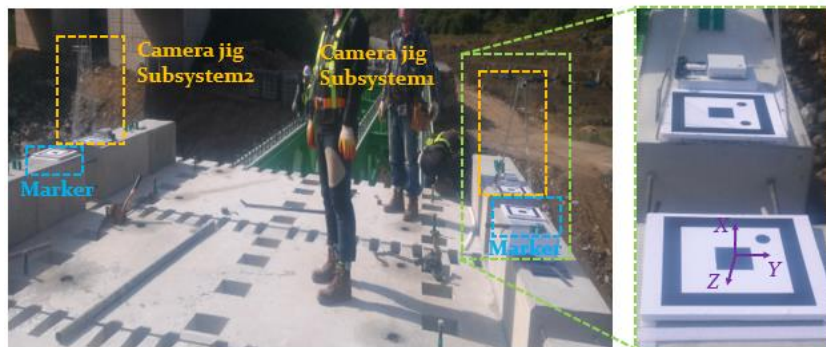


Fig. 23 Coordinate of the fiducial marker

7. Conclusions

To measure the 6-DOF relative displacement of large structures, multiple modules of a camera and a planar marker were suggested, and the hybrid algorithm was developed, which combined the DLT and MCL methods. When the image is not blurred, the experiment was conducted by using a motorized motion-stage to move the camera jig with translation movements of 25 mm, 15 mm, 5 mm, and 0 mm along the X -axis and rotation movements of 0° , 1° , 2° , and 3° about the Z -axis. The largest RMSE of the translation motion was 1.075 mm and that for the rotation about the Z -axis is 0.895 mm. The second experiment showed that when the image is blurred, the RMSE for the hybrid method was 0.739 mm, and the hybrid method was more accurate than the DLT method or MCL method. When the marker was partially hidden in the third experiment, the MCL algorithm could still

estimate the 6-DOF relative displacement, while the DLT algorithm could not. The hybrid method calculated the 6-DOF relative displacement more accurately even when the marker was partially hidden. Finally, the field test showed that the proposed system had a linear error less than a few millimeters, proving our system can accurately estimate 6-DOF relative displacement. In the future work, more field tests and experiments will be conducted to analyze the performance of the proposed system in various weather conditions such as the change of the lighting condition. We will also analyze the performance of the proposed system by conducting various motions of PC members in various assembly conditions. Also, we will redesign camera jigs for the case when the lifting frame is used for assembly. In that case, camera jigs will be installed on the lifting frame because this strategy will eliminate the need for repeated installation of camera jigs every time the PC members are assembled.

Acknowledgments

This research was partly supported by a grant (16SCIP-C116873-01) from Construction Technology Research Program funded by Ministry of Land, Infrastructure and Transport (MOLIT) of Korean government. This research was also supported in part by grant No.10043928 from the Industrial Source Technology Development Programs of the Ministry of Trade, Industry & Energy (MOTIE), Korea. The students are supported by the Korea Ministry of Land, Infrastructure and Transport under the U-City Master and Doctor Course Grant Program.

References

- Abdel, A.Y. and Karara, H. (1971), *Direct Linear Transformation from Comparator Coordinates into Object*, American Society of Photogrammetry, Washington, D.C., USA.
- Caltrans (2004), *Slab replacement guidelines*, State of California Department of Transportation, Sacramento, CA, USA.
- Coppelia Robotics (2016), V-REP <http://www.coppeliarobotics.com/>
- Edwin O. (2011), "AprilTag: A robust and flexible visual fiducial system", *Proceedings of the ICRA (International Conference on Robotics and Automation)*, Shanghai, May.
- Graphics and media lab (2013), *GML camera calibration toolbox*, <http://graphics.cs.msu.ru/en/node/909>.
- Intel Co. (2015a), *OpenCV*, <http://opencv.org/>.
- Intel Co. (2015b), *The introduction of NUC*, <http://www.intel.co.kr>.
- Jeon, H., Bang, Y. and Myung, H. (2011), "A paired visual servoing system for 6-DOF displacement measurement of structures", *Smart Mater. Struct.*, **20**(4), 045019.
- Jeon, H., Choi, S., Shin, J.U., Kim, Y. and Myung, H. (2017), "High-speed 6-DOF structural displacement monitoring by fusing ViSP (Visually Servoed Paired structured light system) and IMU with extended Kalman filter", *Struct. Control. Health Monit.*, **24**(6), e1926.
- Jeon, H., Kim, Y., Lee, D. and Myung, H. (2014), "Vision-based remote 6-DOF structural displacement monitoring system using a unique marker", *Smart Struct. Syst.*, **13**(16), 927-942.
- Jeon, H., Myeong, W., Shin, J.U., Park, J.W., Jung H.J. and Myung, H. (2014), "Experimental validation of ViSP (Visually Servoed Paired Structured Light System) for structural displacement monitoring", *IEEE/ASME T. Mech.*, **19**(5), 1603-1611.
- Jeon, H., Shin, J.U. and Myung, H. (2012), "Incremental displacement estimation of structures using paired structured light", *Smart Struct. Syst.*, **9**(3), 273-286.
- Jeon, H., Shin, J.U. and Myung, H. (2013), "The displacement estimation error back-propagation (DEEP) method for a multiple structural displacement monitoring system", *Meas. Sci. Tech.*, **24**(4), 045104.
- Ji, Y.F. and Chang, C.C. (2008), "Nontarget stereo vision technique for spatiotemporal response measurement of line-like structures", *J. Eng. Mech. - ASCE*, **134**(6), 466-474.
- Lee, D., Jeon, H. and Myung, H. (2012), "Vision-based 6-DOF displacement measurement of structures with a planar marker." *Proceedings of the SPIE (International Society for Optics and Photonics) Smart Structures/NDE*, San Diego, April.
- Lee, D., Jeon, H., and Myung, H. (2014), "Pose-graph optimized displacement estimation for structural displacement monitoring", *Smart Mater. Struct.*, **14**(5), 943-960.
- Lee, J.J. and Shinozuka, M. (2006), "Real-time displacement measurement of a flexible bridge using digital image processing techniques", *Exp. Mech.*, **46**(1), 105-114.
- Logitech Co. (2013), *The introduction of webcam*, <http://www.logitech.com>.
- Marecos, J., Castanheira, M. and Trigo, J. (1969), "Field observation of Tagus river suspension bridge", *J. Struct. Div.-ASCE*, **95**(4), 555-583.
- Myeong, W., Choi, S. and Myung, H. (2015), "Monte Carlo Localization and multiple vision sensor based 6-DOF displacement measurement system for the rendezvous of PC bridge members", *Proceedings of the International Workshop on Structural Health Monitoring*, California, September.
- Myeong, W., Lee, D., Kim, H. and Myung, H. (2014), "Vision-based guide system for rendezvous of PC bridge members using a planar marker", *Proceedings of the 4th International Symposium on Life-Cycle Civil Engineering*, Tokyo, November.
- Myung, H., Lee, S. and Lee, B.J. (2011), "Paired structured light for structural health monitoring robot system", *Struct. Health Monit.*, **10**(1), 49-64.
- Olaszek, P. (1999), "Investigation of the dynamic characteristic of bridge structures using a computer vision method", *Measurement*, **25**(3), 227-236.
- Park, J.W., Lee, J.J., Jung, H.J. and Myung, H. (2010), "Vision-based displacement measurement method for high-rise building structures using partitioning approach", *NDT & E Int.*, **43**(7), 642-647.
- Pheng, L.S. and Chuan, C.J. (2001), "Just-in-time management in precast concrete construction: A survey of the readiness of main contractors in Singapore", *Integ. Manufact. Syst.*, **12**(6-7), 416-429.
- SENA Co. (2015), *User manual of Parani-UD 100*, <http://www.sena.co.kr>.
- The Mathworks, Inc. (2015), *Single Camera Calibration app*, <http://kr.mathworks.com>.
- Thorlabs, Inc. (2015), *Thorlab's V21 photonics catalog*, <http://www.thorlabs.com>
- Thrun, S., Fox, D., Burgard, W. and Dellaert, F. (2001), "Rouster Monte Carlo localization for mobile robots", *Artif. Intell.*, **128**(1-2), 99-141
- Vincent, L., Francese, M.N. and Pascal, F. (2008), "EPnP: An Accurate $O(n)$ Solution to the PnP Problem", *Int. J. Comput. Vision*, **81**(2), 155-166.
- Wahbeh, A.M., Caffrey, J.P. and Masri, S.F. (2003), "A vision-based approach for the direct measurement of displacements in vibrating systems", *Smart Mater. Struct.*, **12**(5), 785-794.
- Yee, A.A. and Chuan, C.J. (2001), "Social and environmental benefits of precast concrete technology", *J. Prestressed Concrete Institute*, **46**(3), 14-19.
- Yuko, U. and Hideo, S. (2007), "Improvement of accuracy for 2D marker-based tracking using particle filter", *Proceedings of the Int'l Conference on Artificial Reality and Telexistence 2007 (ICAT)*, Denmark, November.

HJ